journal

J. Am. Ceram. Soc., 78 [9] 2353-59 (1995)

Surface Cracking in Layers Under Biaxial, Residual Compressive Stress

S. Ho,† C. Hillman,* F. F. Lange,* and Z. Suo

Materials Department, University of California, Santa Barbara, California 93106

Thin two-phase, Al_2O_3/t-$Zr(3Y)O_2$ layers bounded by much thicker $Zr(3Y)O_2$ layers were fabricated by co-sintering powders. After cooling, cracks were observed along the center of the two-phase, Al_2O_3/t-$Zr(3Y)O_2$ layers. Although the Al_2O_3/t-$Zr(3Y)O_2$ layers are under residual, biaxial compression far from the surface, tensile stresses, normal to the center line, exist at and near the surface. These highly localized tensile stresses can cause cracks to extend parallel to the layer, to a depth proportional to the layer thickness. A tunneling/edge cracking energy release rate function is developed for these cracks. It shows that for a given residual stress, crack extension will take place only when the layer thickness is greater than a critical value. A value of the critical thickness is computed and compared with an available experimental datum point. In addition, the behavior of the energy release rate function due to elastic mismatch is calculated via the finite element method (FEM). It is also shown how this solution for crack extension can be applied to explain cracking associated with other phenomena, e.g., joining, reaction couples, etc.

I. Introduction

ATTENTION has been drawn to cracking in layered materials caused by residual stresses, because the problem frequently appears in adhesive joining, electronic packaging, and other technologies. When fabricated at an elevated temperature, T_0, and cooled to T, the two materials that form the layered system studied here suffer a mismatch strain of

$$\varepsilon_M = \int_T^{T_0} (\alpha_2 - \alpha_1)\, dT \tag{1}$$

where α_1 and α_2 are the thermal expansion coefficients of the two materials.

Consider a laminate of a balanced stacking sequence of the two materials so the laminate does not bend. Denote t_1 and t_2 as the thicknesses of layers formed with materials 1 and 2, respectively. Far away from the free surface, the residual stress, σ_R, in each layer is uniform and biaxial. The stress perpendicular to the layers, far from the free surface, is zero ($\sigma_z = 0$). In the layer with the lower thermal expansion coefficient (material 1), the residual, biaxial compressive stress is given by

$$\sigma_{R1} = -\frac{\varepsilon_m E_1'}{1 + \dfrac{t_1 E_1'}{t_2 E_2'}} \tag{2}$$

and in the layer with the greater thermal expansion coefficient (material 2), the biaxial, tensile stress is given by

$$\sigma_{R2} = -\sigma_{R1}\frac{t_1}{t_2} \tag{3}$$

Here $E' = E/(1 - \nu)$, where E and ν are Young's modulus and Poisson's ratio. For the situation where $t_1/t_2 \to 0$, the biaxial stress in material 1 reduces to

$$\sigma_{R1} = -\frac{E_1}{1 - \nu_1}\varepsilon_M \tag{4}$$

and the stress in material 2 vanishes ($\sigma_{R2} \to 0$). For the experimental case considered below, subscripts 1 and 2 distinguish the thinner Al_2O_3/t-$Zr(Y)O_2$ two-phase layers from the thicker t-$Zr(Y)O_2$ layers, respectively. As shown in Table I, $\alpha_1 < \alpha_2$, and thus, biaxial, residual compressive stresses develop within the thinner Al_2O_3/t-$Zr(Y)O_2$ two-phase layers far from the free surface, whereas the much thicker t-$Zr(Y)O_2$ layers are nearly stress free.

It is well known that the stresses at the free surface of layered materials are different from those within the body of the material. Finite element calculations[1,2] show that although biaxial stresses exist far from the surface, a stress perpendicular to the layer plane exists near the free surface that is highly localized, decreasing rapidly from the surface to become negligible at a distance approximately on the order of the layer thickness. This stress has a sign opposite to that of the biaxial stresses deep within the layer. Thus, when the biaxial stresses are compressive deep within the material (case reported below), there is a tensile stress perpendicular to the layer at and near the surface. This reversal of stresses was also observed by Cox[3] during his analysis of inclusions located either within a body or at the surface. Thus, a tensile stress field, localized near the surface, will be present in layers when the stress far from the surface is biaxial compression. These tensile surface stresses can cause the extension of preexisting cracks.

It has been shown that the condition for crack extension within a highly localized stress field depends on both the magnitude of the tensile stress and the size of the body that gives rise to the stress field. This is independent of whether the stress field is residual[4] (e.g., differential thermal expansion) or an applied local stress[5] (e.g., contact stress). Strain energy release rate functions (G) describing the condition for crack extension within thin films and layered materials have been recently reviewed.[6] These functions can be expressed as

$$G = \frac{Z\sigma^2 t}{\bar{E}} \tag{5}$$

where σ is the tensile stress within the film or layer, t is the thickness, $\bar{E} = E/(1 - \nu^2)$, and Z is a dimensionless number that depends on the specific system. Although the topic of surface stresses in embedded layers was not reviewed in Ref. 6, Evans and co-workers[7,8] have analyzed a layered system where a thin metal layer joined two thicker ceramic layers. The thin metal layer was under biaxial tension far from the free surface and its surface was in a state of compression normal to the metal/ceramic interface. Tensile stresses were localized at the surface of the ceramic layers, close to the metal layer, and a strain energy release rate function similar to Eq. (5) was derived to explain the surface cracks observed in the ceramic layers.

M. Thouless—contributing editor

Manuscript No. 192983. Received December 7, 1994; approved April 3, 1995.

Supported by the Defense Advanced Research Projects Agency through the University Research Initiative under the Office of Naval Research Contract No. N-0014-92-J-1808 and the Office of Naval Research Grant No. N00014-90-J-1441.

*Member, American Ceramic Society.

†Present address: Department of Theoretical and Applied Mechanics, University of Illinois, Urbana, Illinois 61801.

Table I. Material Parameters

	α ($\times 10^{-6}$/K)	E (GPa)	ν	Γ (J/m^2)
Al_2O_3/t-Zr(Y)O_2	11.5[23]	300[24,25]	0.32[26,27]	58[23]
t-Zr(Y)O_2	12.5[23]	205[24]	0.32[27]	95[24]

In the present paper, thin alumina–zirconia composite layers were fabricated between two thicker layers of zirconia at high temperature by co-sintering powders. After the laminate cooled to room temperature, a crack was observed along the center line of the alumina–zirconia layer. When the sample was diamond cut normal to the interfaces, similar cracks were observed on all fresh surfaces. Figure 1 shows a schematic diagram and a micrograph. Obviously, the biaxial compressive stress cannot cause cracks in the alumina–zirconia layer. A more careful study reveals that the phenomenon is a surface effect. Near the surface, the stress is nonuniform in each layer and differs from that given in Eq. (4). In particular, the alumina–zirconia layer is under tension in the direction perpendicular to the layer plane. As illustrated in Fig. 2, the thin alumina–zirconia layer strives to contract less than the two zirconia layers, bending its surface and thereby inducing the tensile stress. Consequently, if a condition for crack extension exists due to the tensile stresses near the free surface, the crack should extend only to a certain depth. The purpose of this paper is to use a simplified elastic analysis to determine surface stresses in a layer under residual biaxial

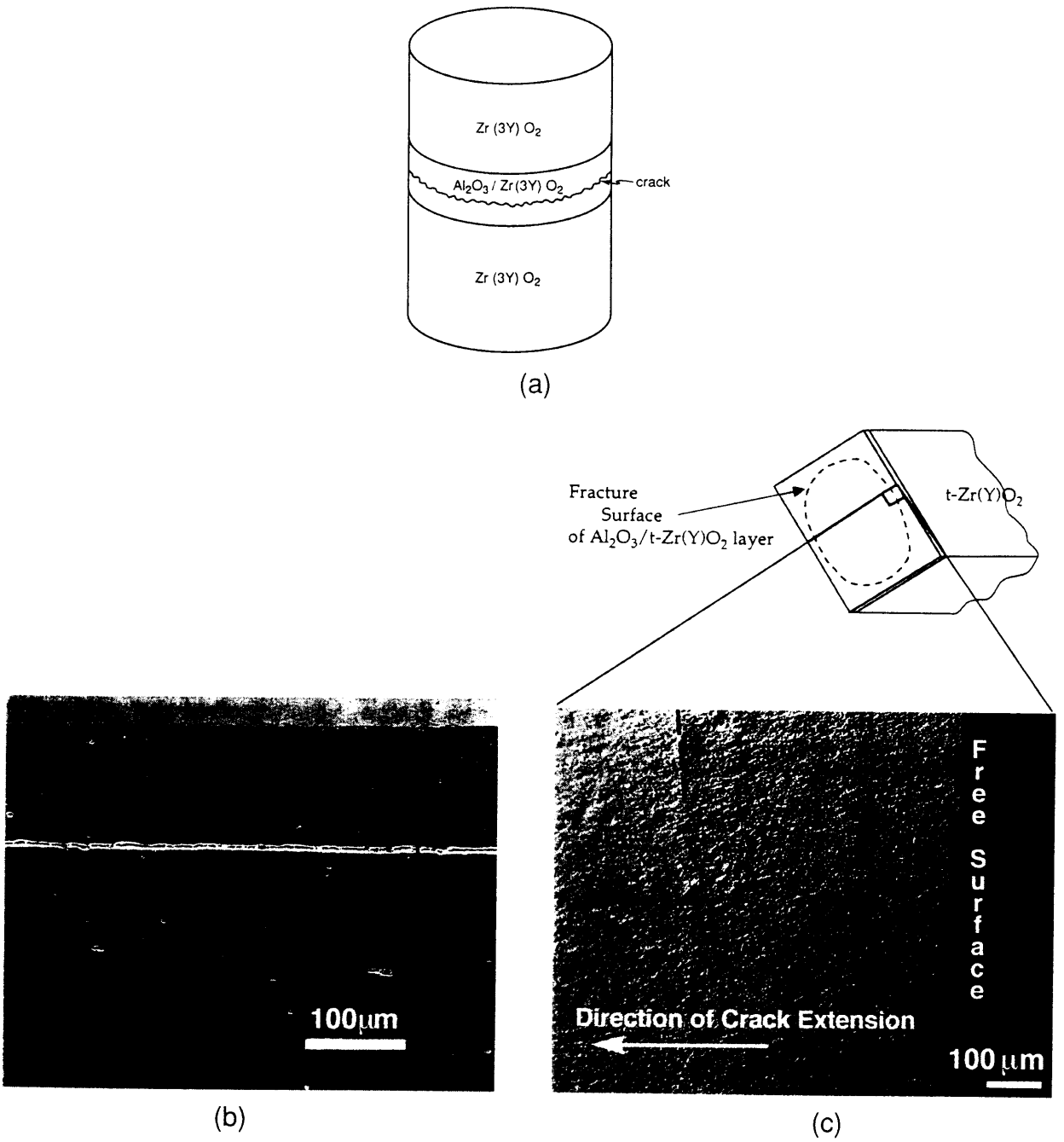

Fig. 1. (a) A thin layer of Al_2O_3/Zr(Y)O_2 is bonded between two blocks of Zr(Y)O_2. A crack runs parallel to the interfaces, in the Al_2O_3/Zr(Y)O_2 layer. (b) An optical micrograph of a crack running in the Al_2O_3/Zr(Y)O_2 layer. (c) SEM micrograph of fracture surface showing sequential positions of the crack front (partial dashed lines) extending from the surface near the center of the Al_2O_3/Zr(Y)O_2 layer.

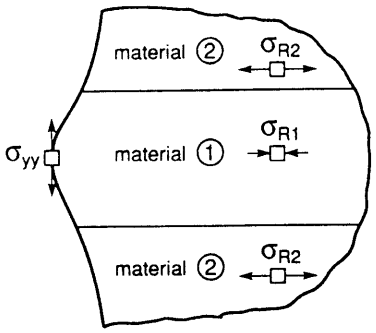

Fig. 2. Far away from the edge, the stress is biaxial in the plane of the laminate, compressive in $Al_2O_3/Zr(Y)O_2$, and tensile in $Zr(Y)O_2$. At the edge, there is a tensile stress normal to the interfaces in $Al_2O_3/Zr(Y)O_2$.

compression far from the free surface, and to show how these surface stresses can induce cracking.

II. Experiments

Microlaminates consisting of thin layers of Al_2O_3/t-$Zr(Y)O_2$ (≈300 μm) sandwiched between thick layers of t-$Zr(Y)O_2$ (≈3000 μm) were fabricated by sequential centrifugation. This method was previously used by Marshall *et al.*[9] to fabricate a new, multilayer laminate with increased fracture toughness. The method utilizes a new colloidal processing technique[10,11] where a short-range repulsive potential is produced by adding salt (e.g., NH_4Cl) to a dispersed, aqueous slurry. The short-range repulsive potential produces a weakly attractive particle network that allows particles to pack to a high relative density by either pressure filtration[10,11] or centrifugation,[12] and prevents mass segregation during centrifugation.[13]

A dispersed, aqueous slurry containing 0.10 volume fraction of t-$Zr(Y)O_2$ powder (TZ-3Y, Tosoh, Tokyo, Japan; ZrO_2 with a tetragonal structure containing 3 mol% Y_2O_3) was prepared at pH 2; 1.0*M* NH_4Cl was then added to create a weakly attractive network. This slurry was used to produce the t-$Zr(Y)O_2$ layers in the laminate. A second slurry, used to produce the layers with a lower thermal expansion coefficient, was prepared to contain 0.005 volume fraction of two powders (0.50 volume fraction Al_2O_3 (AKP-50, Sumitomo Chemical Co., New York) plus 0.50 volume fraction t-$Zr(Y)O_2$ at pH 2 with 1.0*M* NH_4Cl to produce a weakly attractive particle network that prevents phase segregation. A volume V of the appropriate slurry containing the volume fraction of powder, ϕ, was poured into the centrifuge tube, of area A, to form a layer of thickness

$$t = \frac{V\phi}{A}$$

Thus, by varying either the volume fraction of powder in the slurry or the volume poured into the tube, one could vary the desired layer thickness formed during centrifugation. For the current study, the predetermined volume of the t-$Zr(Y)O_2$ slurry was poured into a 50 mL polyethlyene centrifuge tube (Nalgene) and centrifuged at 3200 rpm (centripetal acceleration ~ 1900g) for 2 h (optimum time for maximum particle packing density determined by Ref. 13. The tubes were accelerated slowly up to the highest speed to ensure a smooth surface, and a uniform layer thickness. After centrifugation of the t-$Zr(Y)O_2$ slurry, the clear supernatant was poured off, a predetermined volume of the $Al_2O_3/Zr(Y)O_2$ slurry was introduced into the tube for centrifugation. This process was repeated until the desired number of layers was achieved, i.e., by sequential centrifugation.

The laminates were air-dried and then heated at 2°C/min to 1500°C for 1 h to produce dense laminates. The laminates were sectioned by diamond cutting, polished, and then examined with a scanning electron microscope (SEM) (840 SEM, JEOL, Tokyo, Japan). Cracks, parallel to the interface, were observed near the centerline of the $Al_2O_3/Zr(Y)O_2$ layers (Fig. 1(b)).

To investigate the depth of the cracks, a flexural bar specimen (3.6 mm × 8.5 mm × 20 mm) was prepared such that the thin $Al_2O_3/Zr(Y)O_2$ layer containing the crack was at the center of the bar. When the specimen was loaded in 3-point bending, it failed from the preexisting crack in the thin $Al_2O_3/Zr(Y)O_2$ layer. When the fracture surface was observed in the scanning electron microscope, the position of the crack front prior to catastrophic extension by mechanical testing could be distinguished by a slight change in the crack plane, which clearly marked the crack front. In addition, as shown in Fig. 1(c), several other crack front positions were observed, each apparently caused during cooling by sudden crack extension and arrest. The deepest crack, i.e., the crack front position produced by mechanical fracture, extended from the surface by 550 μm. The thickness of the $Al_2O_3/Zr(Y)O_2$ layer containing the crack was 327 μm, i.e., the normalized crack depth was a/t = 1.68.

III. Mechanics

(1) Stress Distribution Prior to Cracking

The stress given by Eq. (4) prevails inside the alumina–zirconia layer, well away from the surface. Near the surface, the stress distribution is much more complex. To appreciate significant features, we first analyzed a simplified problem. Consider a thin layer of material 1 (thickness t_1) bonded by two much thicker layers of material 2 (thickness t_2), assuming that the two materials have different thermal expansion coefficients but identical elastic constants and that $t_1/t_2 \to 0$. Both materials are fabricated, without bonding, at high temperatures so that their areas are identical before they are cooled. At a lower temperature, the area of the lower expanding material (1) will be larger than the area of material 2. The stress field can be obtained analytically as follows.

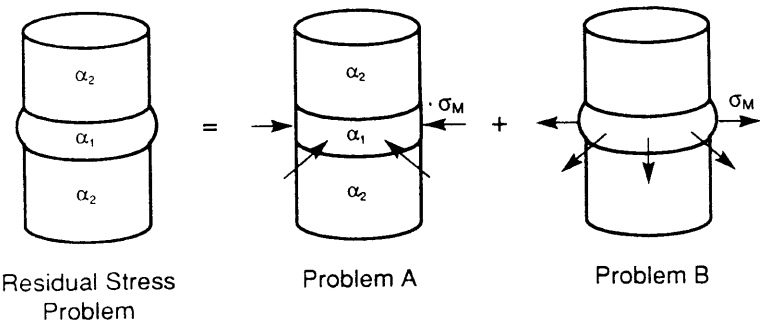

Fig. 3. The residual stress problem is a superposition of the following two problems: (problem A) a band of pressure of magnitude σ_M is applied in addition to the thermal mismatch; (problem B) a band of tensile traction of magnitude σ_M is applied, and there is no thermal mismatch.

The stress induced by thermal mismatch is calculated by superimposing problems A and B in Fig. 3. In problem A, the three layers are detached from one another and a compressive traction of magnitude

$$\sigma_M = \frac{E}{1-\nu}\varepsilon_M \tag{6}$$

is applied at the edge of the thin layer, so that the areas of the two materials are perfectly matched. The stress distribution in problem A is trivial: the two thick layers are stress-free, and the thin layer is under biaxial compression of magnitude σ_M, in the plane of the layer. In problem B, the specimen consists of the three bonded layers, all of which are stress-free; a tensile traction of magnitude σ_M is applied to the thin layer. The superposition of A and B gives just what we want: the stress field induced by the thermal expansion mismatch strain alone, with no surface tractions.

We are interested only in the stress field in the region scaled by the layer thickness; all other lengths—the size of the block and the diameter of the layer—are deemed too large to be relevant. This is a proper assumption for many materials with an embedded layer. Consequently, problem B can be further simplified to be a plane strain problem, i.e., a semi-infinite solid subjected to a band of surface tractions, which is simply a set of point forces along the thickness of the embedded layer (inset Fig. 4). This problem is readily solved by integrating the solution for a point force on a free surface[14] over the band where the tractions are applied. Figure 4 shows the distribution of the stress component σ_{yy} in problem B. This is also the distribution of the residual stress, since the stress component σ_{yy} vanishes in problem A. The centerline of the thin layer coincides with the x-axis. On the surface ($x = 0$), σ_{yy} is a step-function, equal to σ_M in the thin layer, $\sigma_M/2$ at the interface, and zero in the two thick layers. Along the centerline ($y = 0$), the stress is given by

$$\sigma_{yy}(x)|_{y=0} = \frac{2}{\pi}\left[\theta - \frac{1}{2}\sin 2\theta\right]\sigma_M \tag{7}$$

where $\tan\theta = t/2x$. For large depth x, i.e., $\theta \to 0$, this stress decays as

$$\frac{\sigma_{yy}}{\sigma_M} \to \frac{4}{3\pi}\theta^3 \to \frac{1}{6\pi}\left(\frac{t}{x}\right)^3$$

Equation (7) is labeled as $y/t = 0$ in Fig. 4. A similar solution was derived in Ref. 3.

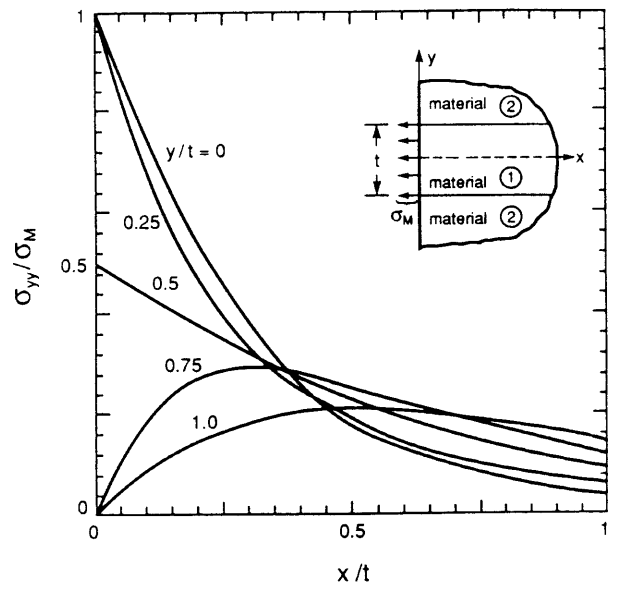

Fig. 4. Distribution of the stress component $\sigma_{yy}(x,y)$ near the edge. The elastic mismatch in this system is assumed to be zero.

The results from Fig. 4 correspond well with the values determined via FEM by Kirchner *et al.*,[2] considering the limitations of FEM for small embedded layers and that Fig. 4 assumes no elastic mismatch.

(2) *Edge and Channel Cracking*

Interacting with preexisting flaws, the tensile stress in Eq. (7) may induce crack extension. Figure 5 illustrates that two situations must be considered; one, the extension of a preexisting crack into the thin layer to a depth a (termed "edging"), and second, the extension of a crack of depth a along the center line of the thin layer (termed "channeling"). Plane strain conditions apply if it is assumed that crack extension into the layer prevails as the crack extends along the center line. The strain energy release rate, G_{ED}, for extension into the layer (edging) is given by[15]

$$\frac{G_{ED}\bar{E}}{\sigma_M^2 t} = \pi\frac{a}{t}s^2\{1.122 - (1-s)\cdot [0.296 + 0.25s^{3/4}(0.75 - s)]\}^2 \tag{8}$$

Here

$$\bar{E} = E/(1-\nu^2)$$

$$s = \frac{2}{\pi}\tan^{-1}\left(\frac{t}{2a}\right)$$

Equation (8) is plotted in Fig. 6 to show that as the crack depth a increases, G_{ED} increases when a is small, reaching the maximum at $a \approx 0.3t$, and then drops when a is large. This trend is expected because the tensile stresses are localized near the surface.

If the critical strain energy release rate of the thin layer material is Γ, then for crack propagation to occur,

$$G_{ED} = \Gamma \tag{9}$$

Graphically, this is analogous to drawing a horizontal line corresponding to Γ normalized by $\bar{E}/\sigma_M^2 t$ in Fig. 6. When the residual stress becomes large enough during cooling, this line will intersect the G_{ED} curve at two points, corresponding to two crack depths. The larger depth is the crack's stable, equilibrium position; it will not grow deeper unless the residual stress increases because of a further decrease in temperature.

The strain energy release rate for channeling, G_{CH}, can be computed using[16]

$$G_{CH} = \frac{1}{a}\int_0^a G_{ED}\,da \tag{10}$$

This result is also plotted in Fig. 6. The overall trends for the two strain energy release rate functions are similar. At $a = 0.55t$, the G_{CH} function reaches its maximum value

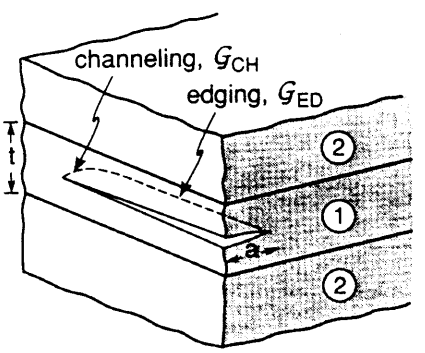

Fig. 5. Two crack fronts: extension deeper into the layer (edging) and spreading around the layer (channeling). The tensile traction σ_M is applied on the surface of layer 1 (not shown in the figure).

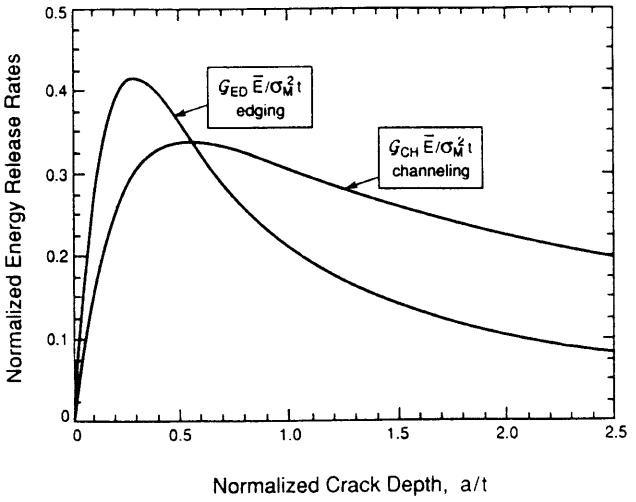

Fig. 6. The energy release rates of edging G_{ED} and channeling G_{CH} vary with the crack depth a. Elastic mismatch is assumed to be zero.

$$(G_{CH})_{max} = \frac{0.34\sigma_M^2 t}{\bar{E}} \tag{11}$$

No preexisting crack can channel along the layer when

$$(G_{CH})_{max} < \Gamma \tag{12}$$

Combining Eqs. (11) and (12), one finds that channeling is possible only when

$$\frac{\Gamma\bar{E}}{\sigma_M^2 t} \le 0.34 \tag{13}$$

Consequently, for a given material pair cooled to a prescribed temperature, there exists a critical thickness, t_c, below which channeling cannot occur, i.e., when

$$t \le t_c = \frac{\Gamma\bar{E}}{0.34\sigma_M^2}$$

The following sequence of events is plausible as a laminate is cooled. The stresses increase from zero during cooling from the fabrication temperature. When the stress is low, favorably oriented, preexisting flaws will neither extend to a greater depth nor channel along the surface. As the stress increases during cooling and reaches the level determined by Eq. (13), a single flaw on the surface, of size around $a = 0.55t$, will be activated to channel along the layer. If the preexisting flaw is much smaller, larger stresses need to develop before the crack spontaneously both extends to a greater depth and channels. After channeling has occurred once, in a catastrophic manner, the crack can extend to greater depths (greater values of a) as the temperature drops further. Because G_{ED} diminishes for large depths, the crack will stabilize at a larger depth determined by Eqs. (8) and (9).

(3) Effect of Elastic Mismatch

When the two materials have different elastic constants, we solve the problem by using the finite element method. As illustrated in Fig. 5, a thin layer of Young's modulus E_1 is bonded between two infinite blocks of Young's modulus E_2. Poison's ratios are taken to be 1/3 for both materials. The elastic mismatch is conveniently described by

$$\frac{E_1 - E_2}{E_1 + E_2} \tag{14}$$

which lies between ± 1, and is positive when material 1 is stiffer than material 2. The thin laminate is loaded by a tensile traction σ_M on the edge of layer 1.

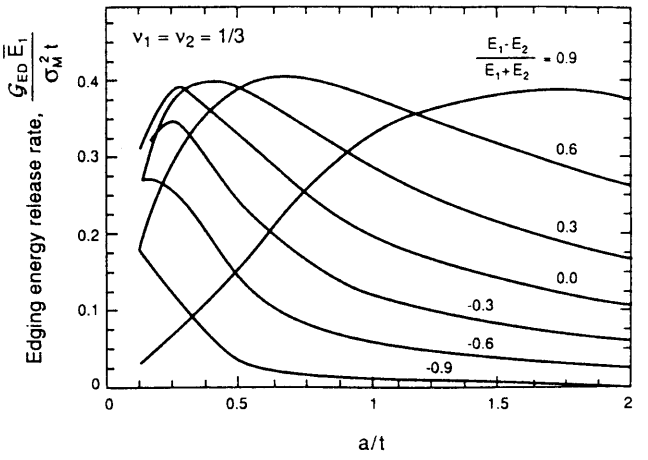

Fig. 7. Edging energy release rate as a function of crack depth and elastic mismatch.

Finite element meshes were generated for various crack sizes, a/t. The accuracy of each mesh was checked by comparing finite element results for $E_1 = E_2$ with the solution presented in the previous section. The calculated strain energy release rates for edging (G_{ED}) are plotted in Fig. 7, where Young's modulus of the thin layer E_1 was used to normalize the energy release rate. Everything else being fixed, as the two thicker layers become more compliant, the curves spread toward the upper right; i.e., the crack will extend deeper into the thin layer.

Once G_{ED} is obtained, one can use Eq. (10) to compute G_{CH}. A more direct approach, more suitable for finite element analysis, is as follows. First the stress distribution $\sigma_{yy}(x)$ on the line of the prospective crack is computed when there is no crack. Then the crack-opening profile, $\delta(x)$, is computed for a traction-free crack. Both computations are done using the finite element method. The channeling energy release rate is calculated by integrating[17]

$$G_{CH} = \frac{1}{2a}\int_0^a \sigma_{yy}(x)\,\delta(x)\,dx \tag{15}$$

The computed results are plotted in Fig. 8. Everything else being fixed, both the maximum, $(G_{CH})_{max}$, and the depth where the maximum occurs increase as the two thicker layers become more compliant.

Crack channeling cannot occur when Eq. (12) is satisfied. The maximum on each curve in Fig. 8 is plotted in Fig. 9 as a function of the elastic mismatch ratio. For a given elastic mismatch, channel cracking is not possible when the dimensionless

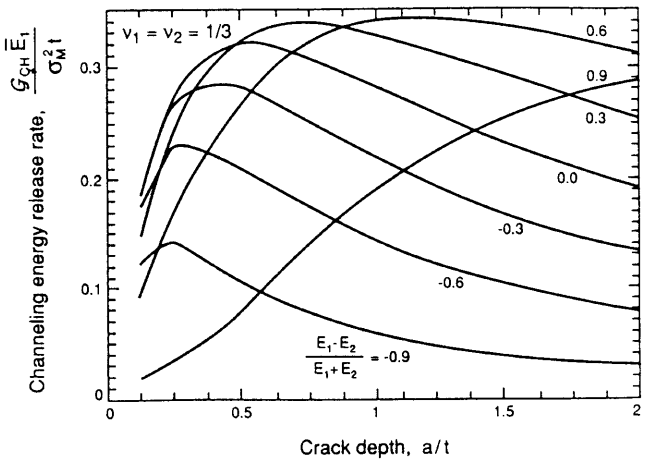

Fig. 8. Channeling energy release rate as a function of crack depth and elastic mismatch.

group, $\Gamma\bar{E}_1/\sigma_M^2 t$, lies above the curve; this region is labeled "no cracking."

IV. Discussion

We have developed an analytical expression for the distribution of tensile stresses at and near the surface of a layer that is under biaxial compression far from the surface. These stresses are consistent with the surface crack observed to bisect the layer. We have also developed critical strain energy release rate functions that describe how far a surface crack will extend into the layer and when it will spontaneously extend along the layer. As for other cases where the tensile stress is highly localized,[1,4–8] it is shown that spontaneous extension along the layer can occur only when the dimensionless group, $\Gamma\bar{E}_1/\sigma_M^2 t$, exceeds a critical value. That is, for a given set of material properties and residual stress, crack extension along the layer will not occur when the layer thickness is less than a critical value.

The strain energy release rate function, Eq. (8), can be tested by comparing the experimental value of the crack depth obtained by observing the fracture surface of the materials used in the current work with the value predicted with Eq. (8). A value of the normalized strain energy release rate of 0.17 is obtained by substituting the experimental crack depth/layer thickness ratio of 1.68 reported above into the right-hand side of Eq. (8) and using a value for the elastic mismatch parameter (Eq. (14)) of 0.2 for the current materials. Using the material properties in Table I, a value of 0.156 was obtained for the left-hand side of Eq. (8). The two values obtained from each side of Eq. (8), 0.17 vs. 0.156, appear to be in sufficient agreement to suggest that Eq. (8) can produce a good estimate for the condition for crack extension, given that the elastic mismatch is small.

The phenomenon described here can be important in many technical situations including the processing and use of multilayer materials, such as capacitors, electronic packaging, piezoelectric actuators, and laminar composites. In these applications, residual stresses arise during the codensification of powder layers due to differential shrinkage, and during cooling from the densification temperature due to differential thermal contraction. For example, in electronic packaging, layers of ceramics and metals are bonded together; the ceramic layers are typically under residual compression far away from the free surface, but under tensile stress at the free surface.

Other important applications include reaction layers formed between two materials at elevated temperatures and bonded joints. Reaction layers can develop between two materials at elevated temperatures. When the reaction product has a larger molar volume, the reaction layer is under biaxial compression far from the free surface but under tension at the surface. An example of this is cited in Ref. 18, where the reaction between nickel and Al_2O_3 produces a spinel layer that results in an extremely weak joint. Since reactions often produce large molar volume changes, and thus, linear strains much larger than those associated with differential thermal expansion, the critical thickness of the reaction layer for spontaneous crack extension can be only a few nanometers; the depth of the crack is expected to increase as reaction proceeds to produce a thicker reaction layer.

Residual stresses can also arise when materials are bonded together with a third material (adhesives, brazes, etc.). In practice, it is well known that the strength of the join depends not only on the magnitude of the residual stress (due to the properties of the third material), but also on the thickness of the joining layer. For example, Kirchner *et al.*[2] have shown that the strength of joints produced between ceramics bonded together with a glass increases with decreasing glass bond thickness, although the maximum tensile stress at the surface was found, by finite element analysis, to be independent of the bond layer thickness. For cases such as these, where a tensile stress is superimposed on the residual tensile stress, the critical bond

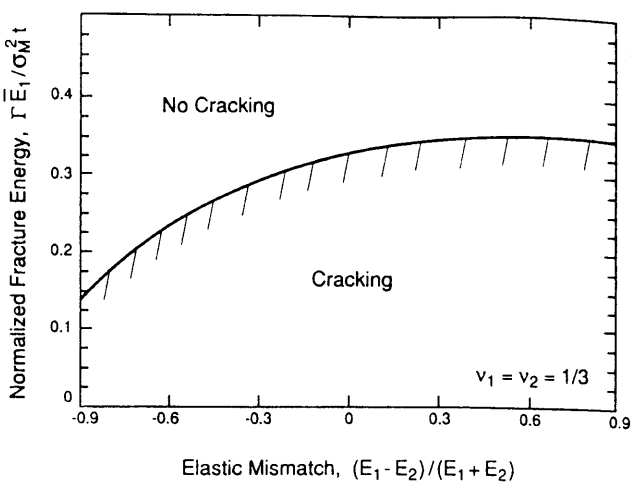

Fig. 9. Condition for the channel cracking to be suppressed.

layer thickness for spontaneous crack extension (i.e., fracture) will depend on the applied to residual stress ratio. Although the critical stress intensity function for this superimposed stress problem is beyond the scope of the present work, its solution is expected to show that the strength of the bonded joint will approach the statistical strength of the ceramic with decreasing bond layer thickness.

Other problems of a similar nature, involving fibers and inclusions under an apparent compressive stress, have been cited in the literature. Cracks have also been observed in fiber-reinforced composites. If fibers have a smaller thermal expansion coefficient than the matrix, the fibers within the matrix are placed under compressive stresses in all three directions during cooling from the processing temperature. However, at the free surface of the composite, tensile stresses develop in the direction normal to the fiber axis. A crack can channel along the fiber if the dimensionless group, $\Gamma E/\sigma_M^2 R$, exceeds a critical number.[19] Here Γ, E, and R are the critical strain energy release rate, Young's modulus, and the radius of the fiber, and σ_M is the mismatch stress.

For inclusions, Lange and Metcalf[20] have shown that cracking due to tensile stresses occurs when an inclusion, nominally under compression when fully embedded in a matrix, is truncated by the surface. For this case, the residual stress in a surface inclusion has been analyzed by Cox[3] as a function of the inclusion shape. Analogous to the surface inclusion, when the surface of a brittle material is suddenly heated in a small region, e.g., when the surface is impinged with a melt droplet or a laser beam, the small region expands. The situation commonly gives a false impression that a compressive stress, parallel to the surface, develops at the heated spot. However, a recent analysis[21] has shown that crack extension can occur due to tensile stress parallel to the surface, under the heated spot.

Finally, it should be pointed out that the stress distribution reported above for free surface of an embedded layer is similar to those imposed by the "bridge" loading method, developed by Nose and Fujii,[22] to introduce a crack of finite depth into a bar specimen. With an appropriate testing method and stress intensity function, the cracked bar is used to determine the critical stress intensity factor of the material. The "bridge" is a slotted block. The bar specimen is compressed between the bridge and a flat surface; except for the region between the slot in the bridge, the opposing surfaces of the bar are compressed. At a critical load, a crack suddenly "pops" into the bar between the slot in the bridge. In this loading configuration, the unloaded region in the bar, defined by the slot in the bridge, is analogous to the layer in the problem analyzed above. That is, localized tensile stresses arise within the bar defined by the slot in the bridge. Similar to the conditions for crack extension in the layer, the crack produced by bridge loading only extends into

the bar to a depth that is proportional to the width of the slot. Thus, although the loading condition is compressive, localized tensile stresses within the unloaded slot region lead to the sudden extension of a crack that arrests at a depth proportional to the width of the slot.

Acknowledgment: Finite element analyses are carried out with ABAQUS.

References

[1]N. L. Harrison and W. J. Harrison, "The Stresses in an Adhesive Layer," *J. Adhes.*, **3**, 195–212 (1972).

[2]H. Kirchner, J. Conway, and A. E. Segall, "Effect of Joint Thickness and Residual Stresses on the Properties of Ceramic Adhesive Joints: I, Finite Element Analysis of Stresses in Joints," *J. Am. Ceram. Soc.*, **70** [2] 104–109 (1987).

[3]B. N. Cox, "Surface Displacements and Stress Generated by a Semi-Ellipsoidal Surface Inclusion," *J. Appl. Mech.*, **56**, 564–70 (1989).

[4]F. F. Lange, "Criteria for Crack Extension and Arrest in Residual Localized Stress Fields Associated with Second Phase Inclusions"; p. 599 in *Fracture Mechanics of Ceramics*, Vol. 2. Edited by R. C. Bradt, D. P. Hasselman, and F. F. Lange. Plenum Press, New York, 1974.

[5]F. F. Lange, "Crack Extension and Arrest for Contact Stress Fields," *Int. J. Fract.*, **12** [3] 409–17 (1976).

[6]J. W. Hutchinson and Z. Suo, "Mixed-Mode Cracking in Layered Materials," *Adv. Appl. Mech.*, **29**, 63–191 (1991).

[7]H. C. Cao, M. D. Thouless, and A. G. Evans, "Residual Stresses and Cracking in Brittle Solids Bonded with a Thin Ductile Layer," *Acta Metall.*, **36** [8] 2037–46 (1988).

[8]M. Y. He and A. G. Evans, "The Strength and Fracture of Metal/Ceramic Bonds," *Acta Metall.*, **39** [7] 1587–93 (1991).

[9]D. Marshall, J. Ratto, and F. F. Lange, "Enhanced Fracture Toughness in Layered Microcomposites of Ce-ZrO_2 and Al_2O_3," *J. Am. Ceram. Soc.*, **74** [12] 2979–87 (1991).

[10]B. V. Velamakanni, J. C. Chang, F. F. Lange, and D. S. Pearson, "New Method for Efficient Colloidal Particle Packing via Modulation of Repulsive Lubricating Hydration Forces," *Langmuir*, **6**, 1323–25 (1990).

[11]J. C. Chang, F. F. Lange, and D. S. Pearson, "Viscosity and Yield Stress of Alumina Slurries Containing Large Concentrations of Electrolyte," *J. Am. Ceram. Soc.*, **77** [1] 19–26 (1994).

[12]J. C. Chang, F. F. Lange, D. S. Pearson, and J. P. Pollinger, "Compaction of Al_2O_3 Slurries by Centrifugation: The Effect of Interparticle Potentials," *J. Am. Ceram. Soc.*, **77** [5] 1357–60 (1994).

[13]J. C. Chang, B. V. Velamakanni, F. F. Lange, and D. S. Pearson, "Centrifugal Consolidation of Al_2O_3 and Al_2O_3/ZrO_2 Composite Slurries vs Interparticle Potentials: Particle Packing and Mass Segregation," *J. Am. Ceram. Soc.*, **74** [9] 2201–204 (1991).

[14]S. P. Timoshenko and J. N. Goodier, *Theory of Elasticity*, 3rd ed. McGraw-Hill, New York, 1970.

[15]H. Tada, P. C. Paris, and G. R. Irwin, *The Stress Analysis of Cracks Handbook*, p. 8.11. Del Research, St. Louis, MO, 1985.

[16]G. Gille, "Strength of Thin Films and Coatings"; Ch. 7 in *Current Topics in Materials Science*, Vol. 12. North-Holland Publishing Co., Amsterdam, Netherlands, 1985.

[17]S. Ho and Z. Suo, "Tunneling Cracks in Constrained Layers," *J. Appl. Mech.*, **60**, 890–94 (1993).

[18]K. P. Trumble and M. Ruhle, "The Thermodynamics of Spinel Interphase Formation at Diffusion-Bonded Ni/Al_2O_3 Interfaces," *Acta Met. Mater.*, **39** [8] 1915–24 (1991).

[19]J. W. Hutchinson; unpublished work.

[20]F. F. Lange and M. Metcalf, "Processing-Related Fracture Origins: II, Agglomerate Motion and Cracklike Internal Surfaces Caused by Differential Sintering," *J. Am. Ceram. Soc.*, **66**, 398–406 (1983).

[21]V. Tvergaard, Z. C. Xia, and J. W. Hutchinson, "Cracking Due to Localized Hot Shock," *J. Am. Ceram. Soc.*, **76**, 729–36 (1993).

[22]T. Nose and T. Fujii, "Evaluation of Fracture Toughness for Ceramic Materials by a Single-Edge-Precracked-Beam Method," *J. Am. Ceram Soc.*, **71**, 328–33 (1988).

[23]C. Hillman and F. F. Lange; unpublished work.

[24]F. F. Lange, "Transformation Toughening, Part 4: Fabrication, Fracture Toughness and Strength of Al_2O_3–ZrO_2 composites," *J. Mater. Sci.*, **17**, 247–54 (1982).

[25]Dr. Dieter Schneider; private communication.

[26]K. Wefers and C. Misra, "Oxides and Hydroxides of Aluminum," Alcoa Laboratories, Pittsburgh, PA, 1987.

[27]B. Eigenmann, B. Scholtes, and E. Macherauch, "Roentgenologic Stress Determination in Ceramics and Metal–Ceramic Composites, Theory and Applications," *Materialwiss. Werksfofftech.*, **20**, 314–25 (1989). □